In-situ Isotopic and Chemical Study of Pyrite from Chu-Sarysu (Kazakhstan) Roll-front Uranium Deposit

Philippe Lach, Michel Cathelineau, Marc Brouand, Nicolas Fiet

Available online at www.sciencedirect.com

ScienceDirect

Procedia Earth and Planetary Science 13 (2015) 207 – 210

Procedia
Earth and Planetary Science

11th Applied Isotope Geochemistry Conference, AIG-11 BRGM

In-situ isotopic and chemical study of pyrite from Chu-Sarysu (Kazakhstan) roll-front uranium deposit.

Philippe Lach[ab], Michel Cathelineau[a], Marc Brouand[c], Nicolas Fiet[c]

[a] *université de Lorraine, CNRS, CREGU, Georessources, Nancy, France*
[b] *BRGM, Orléans, France*
[c] *AREVA Mines, Geosciences Direction*

Abstract

Pyrite is common in roll-front type uranium deposit in Chu-sarysu basin, Kazakhstan. Combined in-situ microstructural, isotopic and chemical analysis of pyrite indicates variation in precipitation conditions and in fluid composition. Broad-scale $\delta^{34}S$ heterogeneity indicates a complex multi-facet evolution. First generation authigenic framboïdal aggregates are biogenic as demonstrated by the lowest $\delta^{34}S$ values of -48‰ to -28‰. The latest generation pyrites are probably hydrothermal with greater $\delta^{34}S$ variation (-30‰ to +12‰). This hydrothermal pyrite commonly displays variable enrichment of several trace elements especially As, Co and Ni. Strong variation in $\delta^{34}S$ values and variable trace element enrichment is interpreted in terms of continuous variations in fluid composition.

Peer-review under responsibility of the scientific committee of AIG-11

Keywords: SIMS, LA-ICP-MS, traces elements, sulfur isotopy, pyrite, uranium, roll-front

1. Introduction

Roll-front uranium deposits in Kazakhstan are characterized by U-bearing minerals systematically mineralized around complex conglomerates of iron sulfides. As pyrite in sands seems to have control on physical and chemical processes for U deposition, they have been separated and studied in detail to define their chemical properties and identify the processes of their formation (bacterial or hydrothermal origin). This study examines pyrite from Chu-Sarysu roll front uranium deposit in Kazakhstan. Microtextural analysis and in-situ microanalysis on a suite of pyrite-bearing samples from a profile across the uranium roll-front provide preliminary constraints on mineralization processes. This study also shows the potential of pyrite to monitor fluid changes in low-temperature hydrothermal systems.

Peer-review under responsibility of the scientific committee of AIG-11
doi:10.1016/j.proeps.2015.07.049

2. Geological context

Roll-Front uranium mineralization of Chu-Sarysu (Kazakstan) occurs in early Paleocene continental arkosic sands issue of peraluminous garnet and calc-alkaline volcanic rocks alteration. These sands were deposited in fluvial environments varying from braided river systems to alluvial plains covered by organic matter rich swamps. The whole sequence has been subject to shallow burial; temperature probably didn't exceed 50°C, and has not evolved since the last deposit. Uranium deposits occur where there is abundant pyrite[6].

3. Methodology

Sixteen samples representing different host formations and redox states were collected along a profile across the roll-front uranium deposit in Kazakhstan. Unconsolidated sands are separated into different size fractions by sieving. Heavy minerals of the fraction between 400 and 63 µm were concentrated using a bromoform solution and set in epoxy one-inch polished ring.

- Optical and scanning electron microscopy (SEM, JEOL J7600F) in back-scattered electron mode (BSE) was used to characterize pyrite morphology and identify relationships with U bearing minerals en Fe-Ti-oxides.
- Laser-ablation (GeoLas 193nm) inductively coupled plasma mass spectrometer (Agilent 7500 cs) was used to obtained trace element concentrations in pyrites. Major element concentration used for internal calibration was providing with electron probe microanalyser (Cameca SX100).
- Isotope analyses of $\delta^{34}S$ were carried out using an IMS 1270 secondary-ion mass-spectrometer (SIMS) on morphologically distinct type of pyrite. Details of analytical methods, for LA-ICP-MS and SIMS are given elsewhere[10,12].

4. Results

4.1. Morphological and textural observations

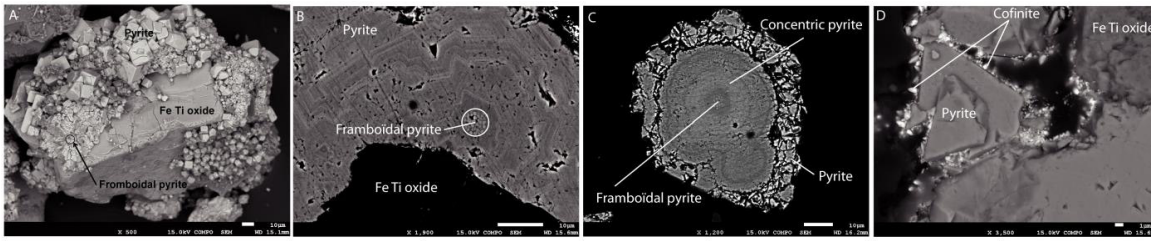

Fig. 1. Back-scattered electron images of pyrites with various morphology and there relations to Fe-Ti oxides and U-bearing minerals. (a) Fe-Ti oxide surrounded by different morphology of pyrite; (b) Polished section of the relation between the different generation of pyrite and Fe-Ti oxide, (c) example of the three main recognizable generation and there relations, (d) zoom on U-bearing mineral mineralized on the surface of pyrite and Fe-Ti-oxides.

Pyrite displays a range of morphologies categorized in this study as: i) framboïdal; ii) concentric and iii) euhedral or cement. The majority of pyrite occur in contact with Fe-Ti oxides (Fig 1, a), and all morphologies are present in all samples.

Framboïds are constituted of densely-packed, spherical aggregates of sub-micrometer-sized pyrite crystals (Fig 1, a, b and c). There can be isolated (Fig 1, c) or clusters of up to several tens of individual framboïds. The framboïds are rarely directly in contact with Fe-Ti oxides. Concentric pyrites exclusively form overgrowths around framboïdal pyrites, and are not found around any other minerals or other pyrite morphology (Fig 1, c). Euhedral or cement pyrite overgrows the two previous generations (Fig 1, c) and frequently link framboidal+concentric pyrite with Fe-Ti oxide (Fig 1 a, b). The morphology of this generation varies widely across the sample suite. Uranium-bearing minerals grow on the surfaces of all types of pyrite and Fe-Ti-oxides (Fig 1, d).

4.2. Trace elements in pyrite and $\delta^{34}S$ values

Traces element analyses have been performed on ten samples. All pyrites are depleted in trace elements. Ti,V, Cu, Zn are detected up to 150ppm for few analysis and below LOD for the most of the analysis. Mo is systematically detected around 40 ppm. Apart these elements, only As, Co and Ni are systematically enriched (up to 14000 ppm for Ni) and are able to discriminate the different generations. Laser spot diameter (and SIMS spot diameter) did not allow specific analysis of the concentric pyrite because of its very small size (10µm max). They are analyzed simultaneously with framboïds and then threated in the same way in Fig. 2.

Arsenic, is moderately concentrated (>500 ppm) in all forms of pyrite (Fig 2a). Some sample more enriched (>1000 ppm) are heterogeneously distributed throughout the sample suite. Co and Ni are less concentrated in framboïdal pyrite (from below detection to 700 ppm with a mean around 120 ppm) than in the other pyrite types (from 100 ppm to 24000 ppm with a mean around 5000 ppm).

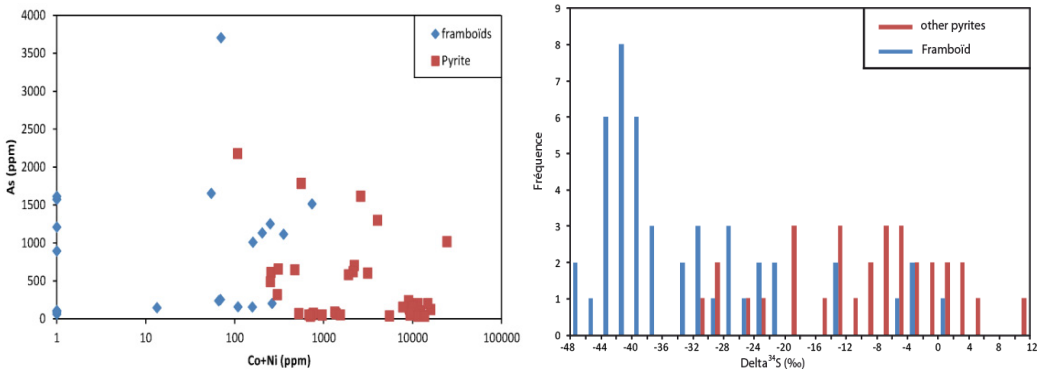

Fig. 2. (a) Distribution of traces elements As and Co+Ni in different morphology of pyrite. (b) $\delta^{34}S$ distribution diagram for different morphology of pyrites (analysis are normalized to Canyon diablo V-CDT value).

$\delta^{34}S$ values from three samples that contain all pyrite types are broadly heterogeneous, ranging between -48‰ and +12‰ (Fig 2b). Framboïd pyrites have lower $\delta^{34}S$ values (-48‰ to -28‰) than other pyrite types which have broader and higher $\delta^{34}S$ values of between -30‰ and +12‰.

5. Discussion

Variation in the traces elements concentration and $\delta^{34}S$ signatures were used to identify geological trends which may impact on understanding of ore genesis.

5.1. Framboïdal pyrite

Framboïdal pyrites in this study are comparable to the distinct aggregates described by Wilkin and Barnes (1997) and may be classified as authigenic[3]. Their large distribution throughout the sample suite and the apparent lack of relationship with Fe-Ti oxides suggest early formation not connected with roll-front formation. This generation of pyrite is poorly endowed in the trace elements Co and Ni as it has been previously observed[3] (Fig 2a). This limited enrichment indicates that the trace elements supplied to the system during authigenic growth were likely supplied by the sandstone host lithology that has low concentrations of traces element. The low $\delta^{34}S$ values (Fig 2b) are similar to those reported by Ingham et al (2013) (between -43.8‰ and -18.3‰) and are characteristic of biogenic formation by bacterial sulfate reduction[7] (BSR).

Indeed while non-organic sulfate reduction produces a sulfate-sulfur isotopic fractionation of around 22‰[2], bacterial processes could induce isotopic fraction of around 46‰[4]. Thus a $\delta^{34}S$ value of around -30 to -40‰ could be expected if the sulfate sources had a $\delta^{34}S$ of around 10 to 20‰ [8]. For lower $\delta^{34}S$ values bacteria may have been able to dismutate elemental sulfur into ^{34}S-enriched sulfate and ^{34}S-depleted sulfide. Unfortunately no data exist about the bacterial population present in this area.

5.2. Concentric pyrite

Because of their small size, concentric pyrites are analyzed simultaneously with framboïdal pyrite with both LA-ICP-MS and SIMS technique. Actually the lack of knowledge on this generation doesn't allow knowing if this generation is biogenic or hydrothermal. But, Folk (2005) shows concentric pyrite formation as a result of bacterial sulfato-reduction. Because this generation is exclusively found around framboïdal pyrite, and because there are as depleted in trace element as the framboïdal pyrite, we can assume that this generation is produce by biogenic processes similarly to framboïdal pyrite.

5.3. Euhedral and cement pyrite

The $\delta^{34}S$ values of late euhedral or cement pyrite are higher than the framboïdal pyrite. The large scattered $\delta^{34}S$ values suggest disequilibrium pyrite mineralization in an open system[7] and suggest hydrothermal mineralization rather than bacterial[5]. Some authors suggest that progressive enrichment of residual fluid in ^{34}S due to preferential incorporation of ^{32}S in framboïdal pyrite coupled with a mixture of several sulfur sources produces scattered $\delta^{34}S$ values in late hydrothermal pyrites[10]. LA-ICP-MS show enrichment in Co and Ni in this last generation suggesting input of these elements during growth of this hydrothermal pyrite[3]. This enhances the hypothesis of fluid evolution during late stage of pyrite formation. Heterogeneous distribution of arsenic across the profile and in all pyrite forms suggest a heterogeneous distribution of fluid across the profile, or/and different sources for As and Co and Ni.

6. Conclusion

Three generations of pyrite were identified. First early and autigenic framboïdal pyrite generation are biogenic and depleted in trace elements suggesting equilibration with poorly evolved fluid. Second generation of concentric pyrite, depleted in trace element and exclusively observable around framboïdal pyrite, could be issue of bacterial process too. Finally the third generation of euhedral or cement pyrite is hydrothermal and surrounds the two other generations. Enrichment in trace element of this generation of pyrite suggests an evolving mineralizing fluids from one or more sources. Micro-scale in-situ textural chemical and isotopic analyses of pyrite highlight the potential ongoing nature of the evolution of the ore system at low temperature.

References

1. Folk, R.L., 2005. Nannobacteria and the formation of framboidal pyrite: Textural evidence. J. Earth Syst. Sci., v. 114, p. 369-374.
2. Harrison, A.G. and Thode, H.G., 1958, Mechanism of the bacterial reduction of sulphate from isotopic fractionation studies: Transactions of the Faraday Society, v. 54, p.84-92.
3. Ingham E, Cook NJ, Cliff J, Ciobanu C, Huddleston A., 2014. A combined chemical, isotopic and microstructural study of pyrite from roll-front uranium deposits, Lake Eyre Basin, South Australia. Geochimica et Cosmochimica Acta 125:440-465
4. Kaplan, I.R., and Rittenberg, S.C., 1964, Microbiological fractionation of sulphur isotopes: Journal of general microbiology, v. 34, p. 195-212.
5. Machel, H.G., 2001. Bacterial and thermochemical sufate reduction in diagenetic settings – old and new insights. Sedimentary Geology, v.140, p. 143-175.
6. Munara A., 2012. Formation des gisements d'uranium de type roll : approche minéralogique et géochimique du gisement uranifère de Muyunkum (Bassin de Chu-Sarysu, Kazakstan). Mémoire de thèse, laboratoire Georessources, Nancy.
7. Seal, R.R., 2006. Sulfur Isotope Geochemistry of Sulfide Minerals. Rev. Mineral. Geochem. V.61, p.633-677.
8. Strauss, H., 1997, The isotopic composition of sedimentary sulfur through time: Palaeogeography, Palaeoclimatology, Palaeoecology, v. 132, p. 97-118.
9. Thomassot, E., Cartigny, P., Harris, J.W., Lorand, J.P., Rollion-Bard, C., Chaussidon, M., 2009. Metasomatic diamond growth: A multi-isotope study (13C, 15N, 33S, 34S) of sulphide inclusions and their host diamonds from Jwaneng (Botswana). Earth and Planetary Science Letters 282, 79-90
10. Warren, C.G., 1972. Sulfur Isotopes as a Clue to the Genetic Geochemistry of a Roll-Type Uranium Deposit. Economic Geology, v. 67, p. 759-767.
11. Wilson S. A., Ridley W. I., Koenig A. E., 2002. Development of sulfide calibration standards for the laser ablation inductively-coupled plasma mass spectrometry technique. J. Anal. At. Spectrom., 17, p406-409.
12. Wilkin R.T. and Barnes H.L., 1997. Formation processes of framboïdal pyrite. Geochimica et Cosmochimica Acta, v. 17, p. 406-409.